Research Article | Vol. 26, No. 16 | 6 Aug 2018 | OPTICS EXPRESS 20111
Optics EXPRESS

Meters-long propagation of diffraction-free space-time light-sheets

BASANTA BHADURI, MURAT YESSENOV, AND AYMAN F. ABOURADDY*

CREOL, The College of Optics & Photonics, University of Central Florida, Orlando, FL 32816, USA
**raddy@creol.ucf.edu*

Abstract: Space-time (ST) wave packets are pulsed beams in which the spatial frequencies and wavelengths are tightly correlated. Proper design of the functional form of these correlations results in diffraction-free and dispersion-free axial propagation; that is, propagation invariance in free space. To date, observed propagation distances of such ST wave packets has been on the order of a few centimeters. Here we synthesize an ST wave packet in the form of a pulsed optical sheet of transverse spatial width ~ 200 μm and spectral bandwidth of ~ 2 nm, and observe its diffraction-free propagation for approximately 6 meters. For such ST wave packets, we identify the *spectral uncertainty*–the precision in associating the spatial and temporal frequencies–as a critical parameter in determining the propagation-invariant distance. We present a design strategy and an experimental methodology that enables further increase in the diffraction-free length.

OCIS codes: (350.5500) Propagation; (050.1940) Diffraction; (320.5540) Pulse shaping.

References and links

1. J. Durnin, J. J. Miceli, and J. H. Eberly, "Diffraction-free beams," Phys. Rev. Lett. **58**, 1499–1501 (1987).
2. D. McGloin and K. Dholakia, "Bessel beams: diffraction in a new light," Contemp. Phys. **46**, 15–28 (2005).
3. M. Mazilu, D. J. Stevenson, F. Gunn-Moore, and K. Dholakia, "Light beats the spread: 'non-diffracting' beams," Laser Photon. Rev. **4**, 529–547 (2010).
4. M. A. Bandres, J. C. Gutiérrez-Vega, and S. Chávez-Cerda, "Parabolic nondiffracting optical wave fields," Opt. Lett. **29**, 44–46 (2004).
5. B. M. Rodríguez-Lara, "Normalization of optical Weber waves and Weber-Gauss beams," J. Opt. Soc. Am. A **27**, 327–332 (2010).
6. G. A. Siviloglou and D. N. Christodoulides, "Accelerating finite energy Airy beams," Opt. Lett. **32**, 979–981 (2007).
7. U. Levy, S. Derevyanko, and Y. Silberberg, "Light modes of free space," Prog. Opt. **61**, 237–281 (2016).
8. J. Turunen and A. T. Friberg, "Propagation-invariant optical fields," Prog. Opt. **54**, 1–88 (2010).
9. H. E. Hernández-Figueroa, E. Recami, and M. Zamboni-Rached, eds., *Non-diffracting Waves* (Wiley, 2014).
10. J. N. Brittingham, "Focus wave modes in homogeneous Maxwell's equations: Transverse electric mode," J. Appl. Phys. **54**, 1179–1189 (1983).
11. L. Mackinnon, "A nondispersive de Broglie wave packet," Found. Phys. **8**, 157–176 (1978).
12. J.-Y. Lu and J. F. Greenleaf, "Nondiffracting X waves–exact solutions to free-space scalar wave equation and their finite aperture realizations," IEEE Trans. Ultrason. Ferroelec. Freq. Control **39**, 19–31 (1992).
13. C. J. R. Sheppard, "Generalized Bessel pulse beams," J. Opt. Soc. Am. A **19**, 2218–2222 (2002).
14. D. N. Christodoulides, N. K. Efremidis, P. Di Trapani, and B. A. Malomed, "Bessel X waves in two- and three-dimensional bidispersive optical systems," Opt. Lett. **29**, 1446–1448 (2004).
15. P. Saari and K. Reivelt, "Evidence of X-shaped propagation-invariant localized light waves," Phys. Rev. Lett. **79**, 4135–4138 (1997).
16. P. Di Trapani, G. Valiulis, A. Piskarskas, O. Jedrkiewicz, J. Trull, C. Conti, and S. Trillo, "Spontaneously generated X-shaped light bullets," Phys. Rev. Lett. **91**, 093904 (2003).
17. H. E. Kondakci and A. F. Abouraddy, "Diffraction-free pulsed optical beams via space-time correlations," Opt. Express **24**, 28659–28668 (2016).
18. K. J. Parker and M. A. Alonso, "The longitudinal iso-phase condition and needle pulses," Opt. Express **24**, 28669–28677 (2016).
19. H. E. Kondakci and A. F. Abouraddy, "Diffraction-free space-time beams," Nat. Photonics **11**, 733–740 (2017).
20. H. E. Kondakci and A. F. Abouraddy, "Airy wavepackets accelerating in space-time," Phys. Rev. Lett. **120**, 163901 (2018).
21. S. Longhi, "Gaussian pulsed beams with arbitrary speed," Opt. Express **12**, 935–940 (2004).
22. P. Saari and K. Reivelt, "Generation and classification of localized waves by Lorentz transformations in Fourier space," Phys. Rev. E **69**, 036612 (2004).

#331320 https://doi.org/10.1364/OE.26.020111
Journal © 2018 Received 21 May 2018; revised 11 Jul 2018; accepted 11 Jul 2018; published 25 Jul 2018

Optics EXPRESS

23. C. Maurer, A. Jesacher, S. Bernet, and M. Ritsch-Marte, "What spatial light modulators can do for optical microscopy," Laser Photon. Rev. **5**, 81–101 (2011).
24. A. Forbes, A. Dudley, and M. McLaren, "Creation and detection of optical modes with spatial light modulators," Adv. Opt. Photon. **8**, 200–227 (2016).
25. A. M. Weiner, "Femtosecond pulse shaping using spatial light modulators," Rev. Sci. Instrum. **71**, 1929–1960 (2000).
26. A. M. Weiner, *Ultrafast Optics* (Wiley, 2009).
27. R. M. Koehl, T. Hattori, and K. A. Nelson, "Automated spatial and temporal shaping of femtosecond pulses," Opt. Commun. **157**, 57–61 (1998).
28. T. Feurer, J. C. Vaughan, R. M. Koehl, and K. A. Nelson, "Multidimensional control of femtosecond pulses by use of a programmable liquid-crystal matrix," Opt. Lett. **27**, 652–654 (2002).
29. B. J. Sussman, R. Lausten, and A. Stolow, "Focusing of light following a $4-f$ pulse shaper: Considerations for quantum control," Phys. Rev. A **77**, 043416 (2008).
30. H. E. Kondakci, M. Yessenov, M. Meem, D. Reyes, D. Thul, S. Rostami Fairchild, M. Richardson, R. Menon, and A. F. Abouraddy, "Synthesizing broadband propagation-invariant space-time wave packets using transmissive phase plates," Opt. Express **26**, 13628–13638 (2018).
31. H. E. Kondakci and A. F. Abouraddy, "Self-healing of space-time light sheets," Opt. Lett. **43**, in press (2018).
32. M. Yessenov, B. Bhaduri, H. E. Kondakci, and A. F. Abouraddy, "Classification of propagation-invariant space-time wave packets in free space: Theory and experiments," unpublished (2018).
33. L. J. Wong and I. Kaminer, "Abruptly focusing and defocusing needles of light and closed-form electromagnetic wavepackets," ACS Photon. **4**, 1131–1137 (2017).
34. L. J. Wong and I. Kaminer, "Ultrashort tilted-pulse-front pulses and nonparaxial tilted-phase-front beams," ACS Photon. **4**, 2257–2264 (2017).
35. A. Sainte-Marie, O. Gobert, and F. Quere, "Controlling the velocity of ultrashort light pulses in vacuum through spatio-temporal couplings," Optica **4**, 1298–1304 (2017).
36. M. A. Porras, "Gaussian beams diffracting in time," Opt. Lett. **42**, 4679–4682 (2017).
37. N. K. Efremidis, "Spatiotemporal diffraction-free pulsed beams in free-space of the Airy and Bessel type," Opt. Lett. **23**, 5038–5041 (2017).
38. M. A. Porras, "Nature, diffraction-free propagation via space-time correlations, and nonlinear generation of time-diffracting light beams," Phys. Rev. A **97**, 063803 (2018).
39. P. Saari, "Reexamination of group velocities of structured light pulses," Phys. Rev. A **97**, 063824 (2018).
40. M. A. Porras, "Self-trapped pulsed beams with finite power in Kerr media excited by time-diffracting, space-time beams," arXiv:1805.07985 (2018).
41. R. J. C. Spreeuw, "A classical analogy of entanglement," Found. Phys. **28**, 361–374 (1998).
42. A. Luis, "Coherence, polarization, and entanglement for classical light fields," Opt. Commun. **282**, 3665–3670 (2009).
43. C. V. S. Borges, M. Hor-Meyll, J. A. O. Huguenin, and A. Z. Khoury, "Bell-like inequality for the spin-orbit separability of a laser beam," Phys. Rev. A **82**, 033833 (2010).
44. A. Holleczek, A. Aiello, C. Gabriel, C. Marquardt, and G. Leuchs, "Classical and quantum properties of cylindrically polarized states of light," Opt. Express **19**, 9714–9736 (2011).
45. X.-F. Qian and J. H. Eberly, "Entanglement and classical polarization states," Opt. Lett. **36**, 4110–4112 (2011).
46. K. H. Kagalwala, G. Di Giuseppe, A. F. Abouraddy, and B. E. A. Saleh, "Bell's measure in classical optical coherence," Nat. Photon. **7**, 72–78 (2013).
47. K. H. Kagalwala, H. E. Kondakci, A. F. Abouraddy, and B. E. A. Saleh, "Optical coherency matrix tomography," Sci. Rep. **5**, 15333 (2015).
48. S. Berg-Johansen, F. Töppel, B. Stiller, P. Banzer, M. Ornigotti, E. Giacobino, G. Leuchs, A. Aiello, and C. Marquardt, "Classically entangled optical beams for high-speed kinematic sensing," Optica **2**, 864–868 (2015).
49. A. Aiello, F. Töppel, C. Marquardt, E. Giacobino, and G. Leuchs, "Quantum-like nonseparable structures in optical beams," New J. Phys. **17**, 043024 (2015).
50. C. Okoro, H. E. Kondakci, A. F. Abouraddy, and K. C. Toussaint, "Demonstration of an optical-coherence converter," Optica **4**, 1052–1058 (2017).

1. Introduction

The demonstration of monochromatic quasi-diffraction-free Bessel beams by Durnin *et al.* [1] fueled tremendous interest in devising optical fields that are propagation invariant [2, 3]. The transverse spatial profile of such beams are eigenfunctions of the Helmholtz equation in various coordinate systems [4–6]; see [7] for a classification of all such solutions. There has been similar interest in synthesizing propagation-invariant *pulsed* beams (or wave packets) that are diffraction-free *and* dispersion-free in free space [8, 9]. Despite the identification of several analytical solutions to the wave equation that satisfy these criteria [10–14], the precise experimental realization of such wave packets has proven to be challenging [15, 16].

Optics EXPRESS

Recent theoretical investigations of propagation-invariant wave packets have helped cast new light on the potential for synthesizing such optical fields, specifically by investigating wave packets having a fixed axial wave number [17, 18]. Subsequently, an experimental strategy for the precise and efficient synthesis of propagation-invariant wave packets in the form of (2 + 1)D pulsed light sheets was devised [19] to produce a variety of wave packets, including hollow beams [19] and non-accelerating Airy wave packets [20] in which one transverse dimension is held uniform. This synthesis approach makes use of the fundamental principle underlying the characteristics of such propagation-invariant wave packets: the existence of tight correlations between the spatial and temporal frequencies constituting the pulsed beam [21, 22], which we thus refer to as 'space-time' (ST) wave packets. Combining techniques from spatial beam modulation [23, 24] and ultrafast pulse shaping [25, 26] carried out jointly with a spatial light modulator (analogous to $4f$ pulse shaping in multidimensional spectroscopy [27–29]) can help produce these unique optical fields. This work has been extended to the synthesis of broadband ST wave packets using refractive phase plates in transmission mode [30], a demonstration of their self-healing properties [31], and a classification of all families of ST wave packets [32]. Furthermore, these recent experimental results have been accompanied by several new theoretical investigations [33–39].

Most previous work has focused on the synthesis and propagation of ST wave packets having narrow spatial profiles, which inherently travel for short distances before diffractive spreading dominates. Typical propagation distances are on the order of a few millimeters or centimeters. For example, in our recent work we demonstrated 7-μm-wide and 14-μm-wide ST wave packets propagating axially for 25 mm and 100 mm, respectively [19]. Achieving such performance requires introducing a tight spectral uncertainty on the order of ~ 30 pm in assigning each wavelength to a spatial frequency.

Here we show that precise spatio-temporal spectral engineering allows for the synthesis of ST wave packets in the form of (2 + 1)D pulsed light sheets that can travel for many meters. After identifying the critical ST wave-packet parameters that dictate its 'propagation-invariant' (or 'diffraction-free') distance, we outline our design strategy to realize the required beam parameters. We find that it is not the size of the spatial profile or spectral bandwidth that solely determine the propagation distance, but that the most influential factor is the width of the *uncertainty* in the spatio-temporal spectral correlations introduced into the field. We synthesize a ST wave packet with the sought-after characteristics, record its spatio-temporal spectral intensity, and confirm its axial propagation invariance over the course of 6 m in agreement with computational predictions.

This paper is organized as follows. First, we describe a theoretical framework for expressing ST wave packets in a plane-wave expansion incorporating judicious spatio-temporal spectral correlations, which also reveals the impact of the spectral uncertainty on the propagation-invariant distance. Based on this framework we design the parameters for a ST wave packet to travel for several meters guided by numerical simulations. We next describe the experimental setup used in the synthesis and characterization of the ST wave packets before presenting our measurement results.

2. Theory

A *generic* (2 + 1)D pulsed beam or wave packet $E(x, z; t) = \psi(x, z; t)e^{i(k_o z - \omega_o t)}$ – in which one transverse dimension is held uniform, $\psi(x, z; t)$ is a slowly varying envelope, and $k_o = \frac{\omega_o}{c}$ is a fixed wave number – has a plane-wave expansion of the form

$$E(x, z; t) = e^{i(k_o z - \omega_o t)} \iint dk_x \, d\omega \, \tilde{\psi}(k_x, \omega - \omega_o) \, e^{i\{k_x x + (k_z(k_x,\omega) - k_o)z - (\omega - \omega_o)t\}}, \qquad (1)$$

where $\tilde{\psi}(k_x, \omega)$ is the two-dimensional Fourier transform of $\psi(x, 0; t)$, x and k_x are the spatial coordinate and component of the wave number in the transverse direction, respectively, z and k_z are the corresponding axial quantities, and c is the speed of light in vacuum. The spatial

Optics EXPRESS

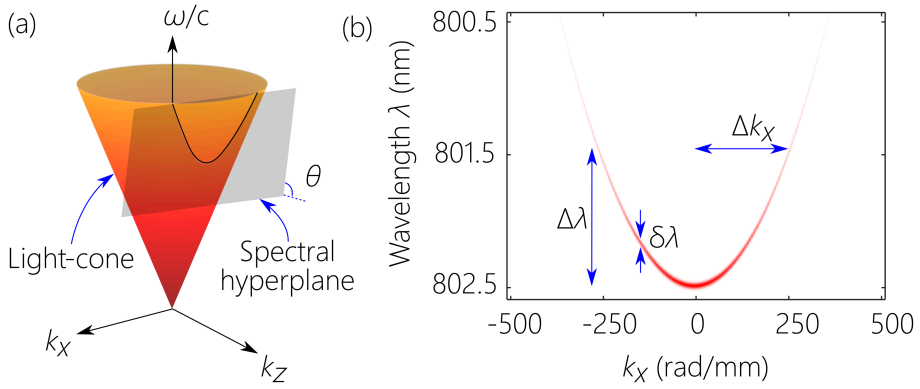

Fig. 1. Concept of a ST light sheet. (a) Geometric representation of the free-space light-cone $k_x^2 + k_z^2 = (\omega/c)^2$. The spectral locus of an ST wave packet lies at the intersection of the light-cone with a spectral hyperplane that is tilted an angle θ with respect to the (k_x, k_z)-plane, is parallel to the k_x-axis, and passes through the point $(k_x, k_z, \frac{\omega}{c}) = (0, k_o, k_o)$. This spectral hyperplane intersects with the $(k_z, \frac{\omega}{c})$-plane in a straight line. (b) Calculated projection of a section of the spatio-temporal spectral curve in (a) onto the (k_x, λ)-plane. The spatio-temporal spectrum has the form of a product of two Gaussian functions, one in k_x and the other in λ whose width is $\delta\lambda$; the temporal bandwidth is $\Delta\lambda = 1$ nm (FWHM), the spatial bandwidth is $\Delta k_x = 250$ rad/mm (HWHM), and $\theta = \frac{\pi}{3}$. The spectral hyperplane intersects with the light-cone in a hyperbola, a section of which is shown here. Note that shorter wavelengths (higher temporal frequencies) are associated with higher spatial frequencies because $\theta > 45°$, in contrast with $\theta < 45°$ (the spectral hyperplane intersects with the light-cone in an ellipse) as used in our experiment, whereupon the association between spatial and temporal frequencies is reversed.

bandwidth is Δk_x and the temporal bandwidth is $\Delta\omega$, which can in general be set *independently* of each other. In free space we have the dispersion relation $k_x^2 + k_z^2 = (\frac{\omega}{c})^2$, which corresponds to the surface of a cone that we refer to henceforth as the 'light-cone'; Fig. 1(a). As such, the spectrum of a generic wave packet is determined by two independent parameters: k_x and ω, the spatial and temporal frequencies, respectively, and k_z is a function of these two variables. The locus of the spatio-temporal spectrum $\tilde{\psi}(k_x, \omega)$ in general is thus a 2D patch on the surface of the light-cone [17, 19].

The propagation-invariant ST wave packets we consider here take an alternate form,

$$E(x, z; t) = e^{i(k_o z - \omega_o t)} \int dk_x \, \tilde{\psi}(k_x) \, e^{i\{k_x x + [k_z(|k_x|) - k_o] z - [\omega(|k_x|) - \omega_o] t\}}, \tag{2}$$

where we now have a one-dimensional spectrum $\tilde{\psi}(k_x)$ with k_x being the only free parameter, and the value of the temporal frequency $\omega(|k_x|)$ – which is no longer an independent parameter – is determined by $|k_x|$. In this setting, k_z is also determined solely by $|k_x|$, and the spatial bandwidth Δk_x is now *correlated* to the temporal bandwidth $\Delta\omega$ [Fig. 1(b)]. The reduction of the number of integrals in Eq. (2) with respect to that in Eq. (1) thus reflects the reduced dimensionality of the spatio-temporal spectrum. By properly engineering the function $\omega(|k_x|)$, we can enforce a *linear* relationship between ω and k_z of the form $\frac{\omega}{c} = k_o + (k_z - k_o) \tan\theta$, where $k_o = \frac{\omega_o}{c}$ is a fixed wave number, and θ is the tilt of this line in the $(k_z, \frac{\omega}{c})$-plane with respect to the k_z-axis. In this case, the wave packet in Eq. (2) takes the form

$$E(x, z; t) = e^{i(k_o z - \omega_o t)} \int dk_x \, \tilde{\psi}(k_x) \, e^{i\{k_x x + [k_z(|k_x|) - k_o][z - ct\tan\theta]\}} \rightarrow e^{i(k_o z - \omega_o t)} \psi(x, z - ct\tan\theta; 0); \tag{3}$$

Optics EXPRESS

in other words, the wave packet has a phase velocity of c and a group velocity of $c\tan\theta$ [21].

The associated spatio-temporal spectral locus of the ST wave packet may thus be viewed as the result of the intersection of the light-cone with a spectral hyperplane that is parallel to the k_x-axis and passes through the point $(k_x, k_z, \frac{\omega}{c}) = (0, k_o, k_o)$; Fig. 1(a). This intersection is a conic section: a circle ($\theta = 0$ and π), an ellipse ($0 < \theta < \frac{\pi}{4}$ and $\frac{3\pi}{4} < \theta < \pi$), a straight line ($\theta = \frac{\pi}{4}$), a hyperbola ($\frac{\pi}{4} < \theta < \frac{3\pi}{4}$), or a parabola ($\theta = \frac{3\pi}{4}$). However, the projection of this conic section on the $(k_z, \frac{\omega}{c})$-plane is *always* a straight line. Moreover, the proportionality between Δk_x and $\Delta\omega$ is also determined by θ. The specific correlation function $\omega(|k_x|)$ is simply the projection onto the $(k_x, \frac{\omega}{c})$-plane of the particular conic section. For example, in Fig. 1(a) where $\theta > 45°$, $\omega(|k_x|)$ is a hyperbola; whereas whenever $\theta < 45°$, $\omega(|k_x|)$ is an ellipse. However, when the spatial bandwidth Δk_x is small, the portion of $\omega(|k_x|)$ exploited in the vicinity of $k_x = 0$ will appear *approximately* as a section of a parabola. In the scenario utilized in our experiments where $\theta < 45°$, the explicit relationship $\omega(|k_x|)$ takes the form of an ellipse,

$$\frac{1}{k_1^2}\left(\frac{\omega}{c} - k_2\right)^2 + \frac{k_x^2}{k_3^2} = 1, \tag{4}$$

where $k_1 = k_o\frac{\tan\theta}{1+\tan\theta}$, $k_2 = k_o\frac{1}{1+\tan\theta}$, and $k_3 = k_o\sqrt{\frac{1-\tan\theta}{1+\tan\theta}}$.

The ideal ST wave packet in Eq. (3) will travel rigidly along z *indefinitely*. Note that the spatial bandwidth Δk_x and the temporal bandwidth $\Delta\omega$ can *both be finite* while retaining the infinite propagation-invariant distance. However, implementing a *delta-function* correlation between k_x and ω requires an infinite aperture, which implies an infinite energy per pulse. In practice, the finite size of the apertures (in particular, of the diffraction grating and the spatial light modulator used in synthesizing the ST wave packet; see below) result in the introduction of a finite uncertainty in the spatio-temporal spectral correlations, which then limits the propagation-invariant distance. In other words, each k_x is no longer associated with a single ω such that $\tilde{\psi}(k_x, \omega) \to \tilde{\psi}(k_x)\delta(\omega - \omega(|k_x|))$. Instead, each k_x is associated with a narrow spectral range $\delta\omega$ centered on $\omega = \omega(|k_x|)$, thereby replacing the delta function with a narrow function $g(\cdot)$ of width $\delta\omega$, such that $\tilde{\psi}(k_x, \omega) \to \tilde{\psi}(k_x)g(\omega - \omega_x)$. We assume that the uncertainty $\delta\omega$, which determines the strength of the correlations introduced into the spatio-temporal spectrum, is smaller than the full temporal bandwidth $\Delta\omega$. The double integral in Eq. (1) is thus regained,

$$E(x, z; t) = \iint dk_x\, d\omega\, \tilde{\psi}(k_x)g(\omega - \omega(|k_x|))\, e^{i(k_x x + k_z(\omega, k_x)z - \omega t)}, \tag{5}$$

but the range of the integration over ω for each k_x is of the order $\delta\omega$.

To appreciate the consequences of the particular form of Eq. (5) for the propagation characteristics of realistic ST wave packets, we make use of a Gaussian spatial spectrum for $\tilde{\psi}(k_x)$ of width Δk_x [Fig. 1(b)] and a Gaussian uncertainty function $g(\omega)$ of width $\delta\omega$ (or $\delta\lambda$ expressed as wavelength) and calculate the propagation-invariant distance L_{ST}. We define L_{ST} as the distance at which the time-averaged intensity $I(x, z) = \int dt|E(x, z; t)|^2$ at the center of the beam $I(0, z)$ has dropped to half its initial value: $I(0, L_{ST}) = \frac{1}{2}I(0, 0)$. In Fig. 2 we plot the result of this calculation as a function of $\delta\lambda$ and Δk_x (or equivalently the transverse width of the spatial profile x_0). Propagation distances ~ 10 m are achievable by *increasing* x_0 (decreasing Δk_x) and *decreasing* $\delta\lambda$. The values of Δk_x and $\delta\lambda$ required to synthesize such ST wave packets are well within our current experimental abilities. The gain in propagation distance can be further increased by continuing this trend in the values of x_0 and $\delta\lambda$; that is, by synthesizing ST wave packets with even larger transverse profiles and/or tighter spatio-temporal spectral correlations.

Optics EXPRESS

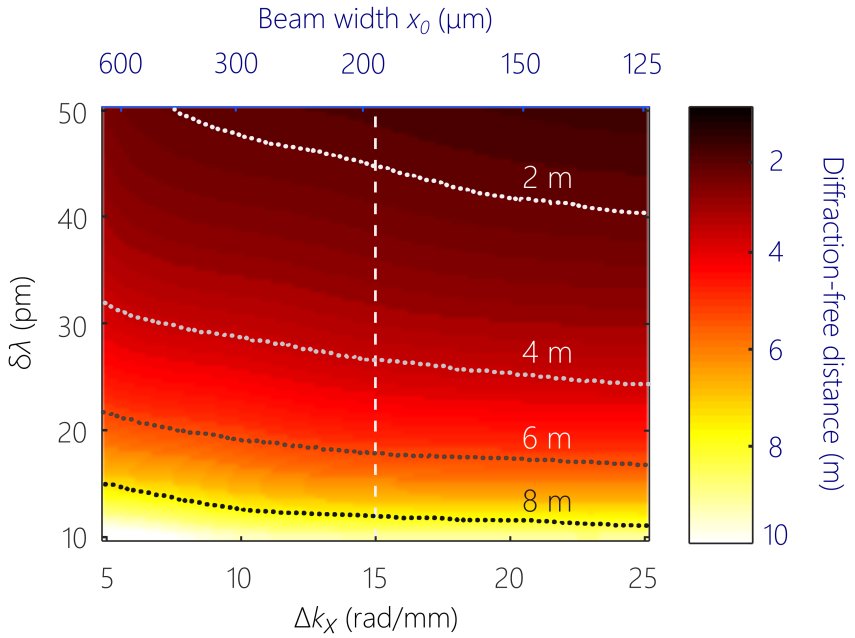

Fig. 2. Calculated diffraction-free (or propagation-invariant) distance for ST light-sheets as a function of spatial bandwidth Δk_x and the spectral uncertainty $\delta\lambda$. The tilt angle of the spectral hyperplane with respect to the light-cone is $\theta = 44.98°$ and the central wavelength is $\lambda_o = 800.5$ nm, which are the values used in our experiment. The spatio-temporal correlations introduced in the ST wave packet entails that the temporal bandwidth $\Delta\lambda$ varies with Δk_x when θ is held fixed. The transverse spatial beam width is $x_0 = \pi/\Delta k_x$.

3. Experimental set-up

The experimental set-up for the synthesis and characterization of the ST light-sheets is shown in Fig. 3, which combines elements from spatial beam modulation and ultrafast pulse shaping. A diffraction grating G (1200 lines/mm; Newport, 10HG1200-800-1) disperses along the y-direction an expanded beam of femtosecond laser pulses (Tsunami, Spectra-Physics; center wavelength of λ_o = 800 nm, bandwidth of $\Delta\lambda$ = 8.5 nm). The second diffraction order is selected and directed to a reflection-mode spatial light modulator (SLM; Hamamatsu X10468-02) through a collimating cylindrical lens L_{1-y}, oriented along y. The SLM imparts a 2D phase pattern $\Phi(x, y)$ to the wave front to jointly modulate the spatial *and* temporal spectra. The nature of this phase distribution is mainly determined by the spectral hyperplane tilt angle θ. Each column on the SLM encodes a linear phase corresponding to a spatial frequency k_x which is then associated with the particular wavelength λ incident at that column. Consequently, arbitrary programmable correlations with one-to-one correspondence between k_x and λ may be introduced into the spatio-temporal spectrum – within a spectral uncertainty $\delta\lambda$ that is determined by the spectral resolving power of the grating and the SLM pixel size. The modulated wave front is retro-reflected back to the grating through the same lens L_{1-y}, whereupon the pulse is reconstituted and all the spatial frequencies are simultaneously overlapped to produce the ST light sheet.

To characterize the ST wave packet behavior, a charge coupled device CCD_1 camera (Imaging Source, DMK 33UX178) records the time-averaged intensity profile $I(x, z)$ along the propagation axis z. Another camera CCD_2 (Imaging Source, DMK 72AUC02) characterizes the spatio-temporal spectrum of the ST light sheet after performing a spatial Fourier transform using a spherical lens L_{2-s}. The combination of lenses L_{1-y} and L_{2-s} forms a $4f$-configuration along y

Optics EXPRESS

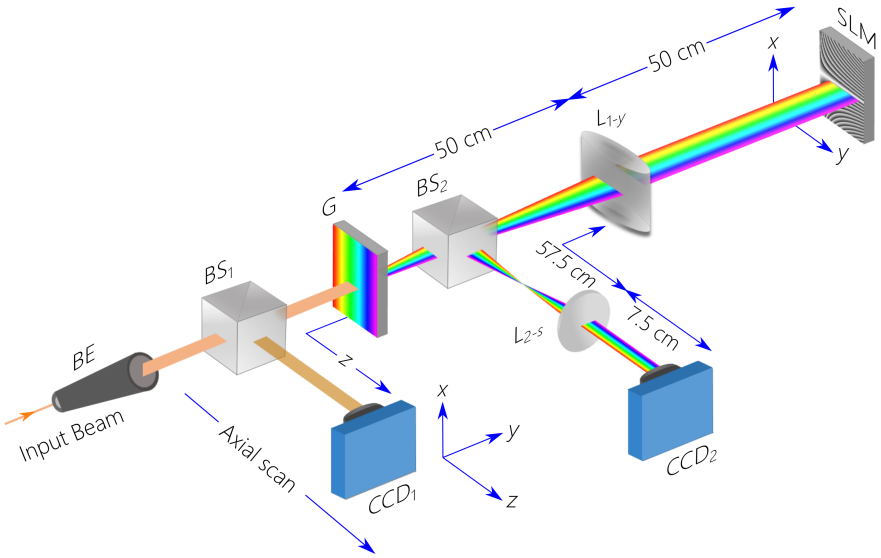

Fig. 3. Schematic depiction of the optical setup for synthesizing ST light sheets. BE: Beam expander; BS_1, BS_2: beam splitters; L_{1-y}: cylindrical lens; L_{2-s}: spherical lens; G: diffraction grating; CCD_1, CCD_2: CCD cameras; SLM: spatial light modulator. The focal lengths of the lenses L_{1-y} and L_{2-s} are 50 cm and 7.5 cm, respectively.

to reproduce the temporal spectrum, while forming a $2f$-configuration along x to produce the spatial spectrum. The spatio-temporal spectrum is thus obtained.

4. Design of the ST wave packet

The design of a propagation-invariant ST wave packet involves the selection of its critical parameters: (1) the spatial bandwidth Δk_x that determines the transverse spatial beam width; (2) the tilt angle θ of the spectral hyperplane [Fig. 1(a)] that determines the temporal bandwidth $\Delta\lambda$ associated with Δk_x and the nature of the conic section on which the spatio-temporal spectrum lies; and (3) the spectral uncertainty $\delta\lambda$ that determines the strength of the spatio-temporal spectral correlations. Selecting the values of these parameters needed to achieve particular propagation characteristics (such as a desired propagation-invariant distance) then guides the synthesis procedure of the ST wave packet by identifying the necessary spatio-temporal spectral correlations to be encoded.

The spectral uncertainty $\delta\lambda$ is limited mainly by the resolving power of the diffraction grating [Fig. 3], although the sizes of the remaining apertures in the optical system may also play a similar role. The spectral resolving power of a diffraction grating at a wavelength λ is given by $R=\lambda/\delta\lambda=m*N$, where m is the diffraction-order selected, N is the total number of illuminated grating lines (groove-frequency $\times$ grating-length), and $\delta\lambda$ is the spectral resolution. This formula, however, is derived with the assumption that the incident field has a flat intensity profile at the grating. The use of a Gaussian beam leads to an increase in $\delta\lambda$. In our experiment, we made use of a diffraction grating with 1200 line/mm and dimensions of 25×25 mm^2, which gives a lower limit on the spectral uncertainty of $\delta\lambda\approx14$ pm for the second diffraction order $m=2$. Gratings with a higher density of rulings would provide a stronger resolving power, but at the expense of lower diffraction efficiency at the operating wavelength $\lambda=800$ nm. Similarly, exploiting higher diffraction orders enhances the spectral resolving power but reduced the diffraction efficiency. The limit of the spectral resolution measurable in our optical spectrum analyzer is 30 pm. However,

Optics EXPRESS

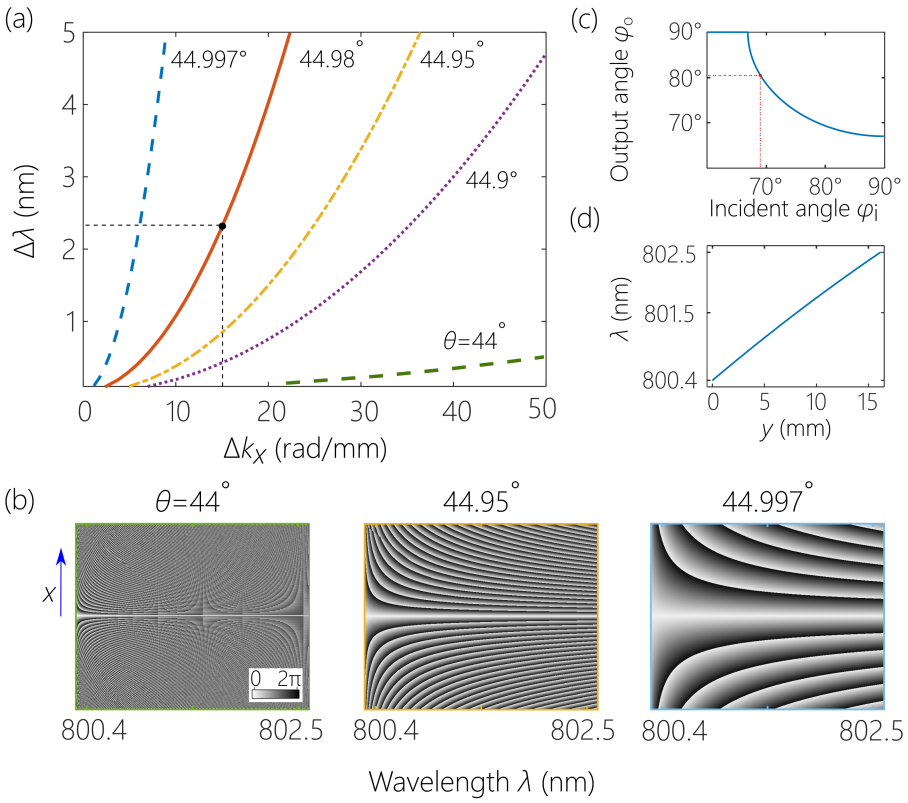

Fig. 4. Selection of the parameters of the ST light sheet. (a) Dependence of the temporal bandwidth $\Delta\lambda$ on the spatial bandwidth Δk_x for 5 different tilt angles θ in the range $44° \le \theta < 45°$. (b) Phase patterns displayed on the SLM for three tilt angles from (a). The point at $k_x = 15$ rad/mm for $\theta = 44.98°$ is the operating point in the experiment. (c) The relationship between the incidence angle φ_i and output angle φ_o of the second diffraction order $m = 2$ for the diffraction grating G in Fig. 3. The dotted lines identify the selected parameters in our experiment. (d) The spatial distribution along the y-direction of the wavelengths at the SLM plane for an incidence angle of $\varphi_i = 69°$ on the grating, as highlighted in (c).

the parameters of our setup support that the actual value is ≈25 pm.

After determining the achievable spectral uncertainty $\delta\lambda$, we refer to the calculations plotted in Fig. 2 to estimate an upper value for Δk_x to achieve a propagation distance of several meters. We choose $\Delta k_x \approx 15$ rad/mm, corresponding to a propagation distance estimated at 6 m. The next step is the selection of an appropriate angle θ for such a small value of Δk_x (with respect to those in [19, 20, 30–32]), which in turn dictates the associated temporal bandwidth $\Delta\lambda$. We plot in Fig. 4(a) the relationship between Δk_x and $\Delta\lambda$ for different values of θ in the range $44° \le \theta < 45°$. Relying on values of θ approaching 45° has the advantage of requiring a larger $\Delta\lambda$, which enables us to efficiently utilize the source bandwidth (8.5 nm). Taking these facts into consideration, we choose an angle $\theta = 44.98°$, which requires a bandwidth of $\Delta\lambda \approx 2$ nm. The required SLM phase pattern $\Phi(x, y)$ is shown in Fig. 5(a). It may initially seem that such precise control over θ presents an exorbitant experimental challenge; specifically, in designing the SLM phase pattern $\Phi(x, y)$. However, small changes in θ in the vicinity of $\theta = 45°$ produce large changes in $\Phi(x, y)$. A few examples are shown in Fig. 4(b) corresponding to three of the values of θ in Fig. 4(a).

Optics EXPRESS

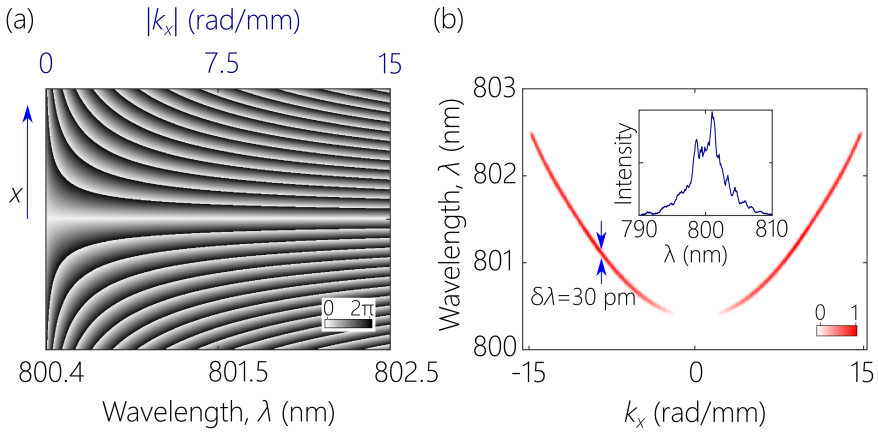

Fig. 5. Synthesis of ST light sheets. (a) The phase distribution $\Phi(x, y)$ imparted by the SLM onto the impinging spatially spread spectrum to produce the target ST light sheet. (b) Measured spatio-temporal spectrum $|\tilde{E}(k_x, \lambda)|^2$ obtained by CCD_2. The inset shows the spectral intensity of the initial femtosecond Ti:Sa pulses.

The last experimental parameter to be selected is the incidence angle of the laser onto the diffraction grating, which is selected to optimally spread the required bandwidth ($\sim$2 nm) along the width of SLM (16 mm). Based on the plot of diffracted angle ϕ_o of the second diffraction order versus the incident angle ϕ_i in Fig. 4(c), we select $\phi_i \approx 69°$, which results in a wavelength spread across transverse coordinate shown in Fig. 4(d). A total temporal bandwidth of $\sim$2.1 nm from the original laser spectrum is modulated along the 16-mm-wide SLM.

5. Experimental results

In order to confirm the diffraction-free behavior of the ST light sheet in physical space (x, z), we recorded the time-averaged intensity profile $I(x, z)$ along the z-direction for 6 m using CCD_1 [Fig. 3]. This long distance is scanned by CCD_1 via a series of mirrors that fold the beam back and forth on an optical table. Note that specular reflections from surfaces do *not* affect the spatio-temporal correlations encoded in the wave packet, and thus do not change the propagation-invariant characteristics.

Towards this end, the phase pattern shown in Fig. 5(a) is imparted by the SLM to the spread spectrum, which corresponds to the operating point in Fig. 4(a). This phase pattern is based on the spatio-temporal trajectory on the light-cone resulting from selecting the angle $\theta = 44.98°$. The measured spatio-temporal spectrum $|\tilde{E}(k_x, \lambda)|^2$, which is the squared modulus of the 2D Fourier transform of $E(x, 0; t)$, is plotted in Fig. 5(b). The measurement confirms that (a) the temporal bandwidth is indeed $\sim$2 nm extracted from the original spectrum of the Ti:Sa pulses, shown in Fig. 5(b), inset; and (b) that the associated spatial bandwidth Δk_x is the predicted value for the selected θ. The (k_x, λ)-curve in Fig. 5(b) appears as a parabola because of the small value of Δk_x implemented, but it is actually a section of the ellipse described in Eq. (4).

Such a choice produces a ST light sheet whose full width at half maximum (FWHM) is $x_0 \approx 183$ μm at $z = 0.5$ m, which increases to ≈ 339 μm after propagating a distance of $z = 6$ m. Note that the Rayleigh range of a Gaussian beam of same initial transverse width is $z_R \approx 13.15$ cm. Figure 6(a) shows the transverse intensity profiles at $z = 0.5$ m, $z = 1$ m, and subsequently in 1-m increments to $z = 6$ m. The increase in the width of the ST wave packet upon free propagation is shown in more detail in Fig. 6(b) along with the drop in the peak on-axis intensity $I(0, z)$ in Fig. 6(c). The observed axial range corresponds to $\approx 45 z_R$. We note that a slight rotation of the

Optics EXPRESS

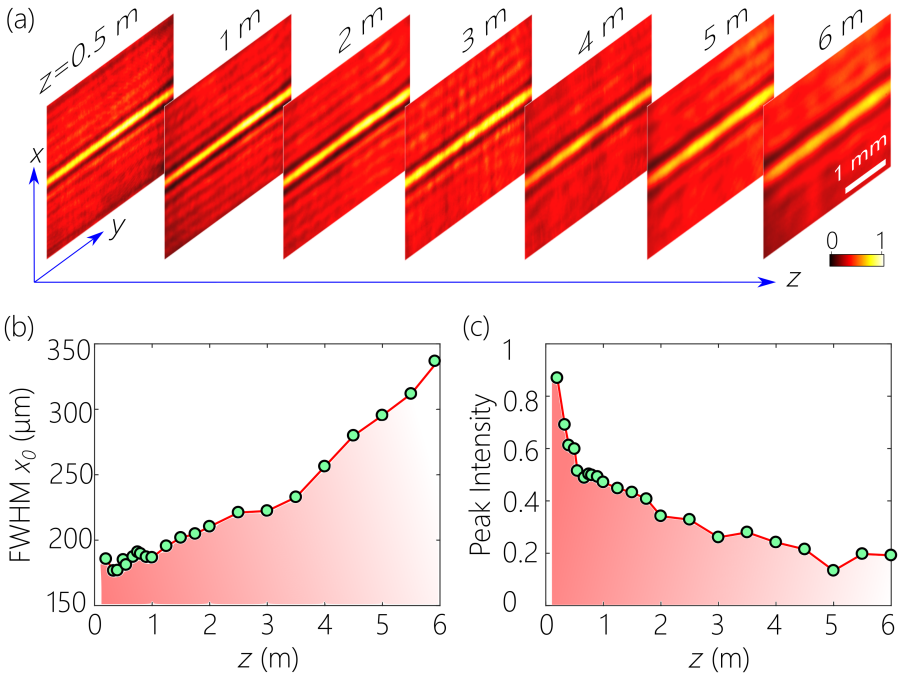

Fig. 6. (a) Measured spatial profiles $I(x, y; z)$ at selected axial positions z (provided above each panel) extending up to 6 m. The scale bar represents 1 mm along both x and y directions. (b) Evolution of the transverse FWHM of $I(x, z)$ and (b) the peak intensity $I(0, z)$ along the axial direction z.

plane of the ST light-sheet was observed along the propagation axis on the order of 2° over a distance of ≈ 4 m. This is likely due to remaining slight relative misalignments between the diffraction grating, lens L_{1-y}, and SLM in which the rotational symmetry around the propagation axis is broken.

6. Conclusion

In conclusion, we have synthesized a diffraction-free (2 + 1)D ST wave packet in the form of a pulsed light-sheet that travels in free space for an axial distance of ~ 6 m. Precise spatio-temporal spectral engineering enables the synthesis of a pulsed beam in which each spatial frequency underlying the transverse beam profile is precisely associated with a temporal frequency underlying the pulse linewidth. Utilizing an SLM-based optical arrangement that combines elements of spatial beam modulation and ultrafast pulse shaping, we produce an ST wave packet of transverse width ~ 200 μm that travels for at least 6 m. Paramount to achieving this performance is control over the spectral uncertainty in the association between spatial and temporal frequencies.

Another critical factor in the wave packet design is the judicious selection of the tilt angle of the spectral hyperplane – that contains the spatio-temporal spectrum of the wave packet – with respect to the light-cone. These results indicate that it is possible to utilize ST wave packets for extended distances. Combined with the potential for synthesizing high pulse-energy ST wave packets via refractive phase plates [30], applications in laser filamentation may become possible [40]. This requires first extending the experimental approach described here to (3 + 1)D ST wave packets that are localized in all dimensions.

Finally, we note that the spatio-temporal spectral correlations introduced into the ST wave packets are the continuous analog of the correlations between discrete degrees of freedom

Optics EXPRESS

(such as polarization and spatial modes) in what has recently come to be known as 'classical entanglement' [41–50]. The strength of these correlations between the spatial and temporal degrees of freedom of the optical field, or the degree of classical entanglement, is determined by the width of the spectral uncertainty. As such, the degree of classical entanglement dictates the propagation-invariant distance of ST wave packets.

Funding

U.S. Office of Naval Research (ONR) contract N00014-17-1-2458.

Acknowledgment

We thank D. Mardani, G. K. Atia, and H. E. Kondakci for helpful discussions.